Energy Storage Materials 27 (2020) 198–204

Contents lists available at ScienceDirect

Energy Storage Materials

journal homepage: www.elsevier.com/locate/ensm

Suppressed dendrite formation realized by selective Li deposition in all-solid-state lithium batteries

Xiaofei Yang [a,1], Xuejie Gao [a,1], Changtai Zhao [a], Qian Sun [a], Yang Zhao [a], Keegan Adair [a], Jing Luo [a], Xiaoting Lin [a], Jianneng Liang [a], Huan Huang [c], Li Zhang [b], Shigang Lu [b], Ruying Li [a], Xueliang Sun [a,*]

[a] Department of Mechanical and Materials Engineering, University of Western Ontario, London, ON, N6A 5B9, Canada
[b] China Automotive Battery Research Institute, Beijing, 100088, PR China
[c] Glabat Solid-State Battery Inc., 700 Collip Circle, London, ON, N6G 4X8, Canada

ARTICLE INFO

Keywords:
Solid-state electrolyte
Selective deposition
Solid polymer electrolyte
Lithium batteries
Li dendrite

ABSTRACT

Solid polymer electrolytes (SPEs)-based all-solid-state lithium batteries (ASSLBs) with high-safety and high-performance have been regarded as promising next-generation energy storage devices. A fly in the ointment is that the cycling life is significantly limited by the Li dendrite growth. To tackle the Li dendrite issue, a selective Li deposition strategy is proposed, for the first time, to suppress Li dendrite formation via the rational design of a patterned Li anode. Through a facile and low-cost template-press method, the Li anode was divided into numerous square Li with deep grooves around 100 μm. Benefiting from the focused current density in the grooves, the Li preferentially deposits in the grooves instead of on the surface, thus suppressing the Li dendrite formation during the Li plating/stripping process. With this in mind, both cycling life of the assembled Li–Li symmetric cells and Li–$LiFePO_4$ (LFP) full cells is prolonged for over 5 times. The Li–Li symmetric cells assembled with the patterned Li exhibit excellent cycling stability for 800/400 h at 0.1/0.2 mA cm^{-2}. More importantly, the 3–4 mg cm^{-2} LFP-loaded patterned Li/PEO/LFP cell achieves high capacity retention of 91.3% within 100 cycles at 0.5C, while different degrees of short-circuits occurred for the bare Li/PEO/LFP cells.

1. Introduction

High-safety and high-energy-density all-solid-state lithium batteries (ASSLBs) have attracted intense interest recently [1–4]. Among various solid-state electrolytes (SSE), solid polymer electrolytes (SPEs) with high-flexibility, easy fabrication and low cost have been regarded as one of the most promising candidates closest to the practical application [5–9].

However, most SPEs present low mechanical strengths at operating temperatures, which significantly hinder their practical application in ASSLBs due to the Li dendrite growth [10,11]. To tackle the aforementioned issue, tremendous efforts have been focused on improving the mechanical properties of SPEs. The most widely adopted two strategies are the introduction of inorganic fillers with high modulus and fabrication crosslinking polymer networks. Such inorganic metal/non-metal oxides as Al_2O_3 [12], SiO_2 [13], oxide-based SSEs like LLZO [14–16], LATP [17,18] were introduced into the SPEs to enhance the ionic conductivity as well as suppress Li dendrite growth. For instance, Garnet-type $Li_{6.75}La_3Zr_{1.75}Ta_{0.25}O_{12}$ (LLZTO) with an ultra-high shear modulus of 55 Gpa was developed as an effective filler into the PEO matrix, which played important roles in enhancing the mechanical strength and inducing uniform Li^+ distribution on the surface of Li anode as well, thus improved the Li dendrite suppression capability [19]. Nevertheless, the discontinuity of the particle fillers dispersed in the polymer matrixes shows the inability to suppress Li dendrite effectively. To tackle this issue, fabrication of 3D interconnected scaffolds via electrospinning [20], aerogel [21], hydrogel [22] and template methods [23] for polymer infusion has been developed as an alternative. Very recently, our group proposed to impregnate the PEO electrolyte into commercially available glass fibers, which significantly enhanced the mechanical strength of the SPE, even under a high temperature of 120 °C. The assembled Li–Li symmetric cells demonstrated excellent cycling stability for over 1000 h at a current density of 0.42 mA cm^{-2} (capacity:0.4 mAh

* Corresponding author.
E-mail address: xsun9@uwo.ca (X. Sun).
[1] Those authors contributed equally to this work.

https://doi.org/10.1016/j.ensm.2020.01.031
Received 11 November 2019; Received in revised form 22 December 2019; Accepted 29 January 2020
Available online 1 February 2020

cm^{-2}) [24].

Alternatively, the fabrication of a polymer network via cross-linking strategy has also been verified to be effective in enhancing the mechanical strength of SPEs. For instance, a high mechanical strength of 12 GPa was realized by Guo's group via photopolymerizing a branched acrylate onto the ion-conductive PEO matrix, which was strong enough to inhabit Li dendrite growth and achieved 130 h cycling life of assembled Li–Li symmetric cells at a high current density of 4 mA cm^{-2} [25]. Besides, electrolyte additives were developed to stabilize the Li anode surface to suppress the Li dendrite growth. In situ formation of Li_3N on the surface of Li metal by introducing LiN_3 into the SPE exhibited excellent cycling stability of over 650 h at 0.1 mA cm^{-2} (capacity:0.2 mA cm^{-2}, which is over 6 times longer than that of LiN_3-free counterpart [26]. In another study, a self-healing electrostatic shield (SHES) mechanism was proposed by Sun's group by adding less than 1 wt% Cs^+ into PEO electrolytes and prolonged the Li–Li symmetric cells' life for almost one order of magnitude [27].

It should be noted that most strategies mentioned above are based on the SPE modification. Nevertheless, several challenges were still remained such as worsening energy density with the introduction of high-mass-density oxide fillers, time-consuming cross-linking process as well as the degradation of Li dendrite suppression capability because of electrolyte additives consuming during the plating/stripping process. In this regard, it is necessary to further explore more Li dendrite suppression methods based on both Li surface modification and SPEs decoration. Herein, a selective Li deposition strategy was proposed, for the first time, by constructing a patterned Li anode in SPE systems. The focused current density forced Li selectively deposited in the patterned grooves, which suppresses the Li dendrite formation. As a consequence, both the Li–Li symmetric cells and Li-LFP full cells assembled with patterned Li demonstrated over 5-times longer cycling life compared with the bare Li. The rational structure design of patterned Li will offer an opportunity for enhancing the metal dendrite suppression capability in other solid-state batteries such as Li/Na–S and Li/Na–O_2 as well as Na-ion batteries.

2. Experimental section

2.1. Fabrication of patterned Li

The patterned Li was prepared by a template-press method. Firstly, a stainless steel mesh (SSM) was put on the surface of a Li foil and then added an external pressure of 30 kg cm^{-2} and kept for 10s. Then removing the SSM, a patterned Li with a grid structure was obtained.

2.2. Synthesis of PEO electrolyte

The PEO electrolyte was prepared by a solution casting method. Firstly, the mixed solution of PEO polymer (M_w: 1000000, 0.60 g), bis(trifluoromethylsulfonyl) imide (LiTFSI) salt (0.24 g) were dissolved in 20 mL acetonitrile and vigorous stirring overnight, where the EO/Li ratio was controlled as 16/1. Then, the solution was cast in a polytetrafluoroethylene (PTFE) dish and dried at 60 °C for 24 h in vacuum. The obtained polymer membrane was labeled as the PEO electrolyte.

2.3. Synthesis of $LiFePO_4$ (LFP) electrodes

The LFP electrodes were fabricated by a blade-casting technique. Typically, the LFP powder, acetylene black and PEO/LITFSI (EO/Li = 16/1) was dissolved in acetonitrile with a weight ratio of 8:1:1 to form a slurry and then coated onto aluminum (Al) foil. After that, the Al foil coated with slurry was directly dried in a 60 °C oven overnight. The obtained cathodes were labeled as LFP electrodes.

2.4. Materials characterization

The morphology, structure, and composition of the PEO electrolyte and Li anode were characterized by SEM (Hitachi S-3400). Due to inseparability between the PEO electrolyte and patterned Li/bare Li after plating/stripping, low molecular PEO (Mw = 4000) infused into a Celgard 3501 membrane was applied as the electrolyte for the Li deposition behavior study. After the disassembly of the cells, the patterned Li/bare Li was washed with 1,2-dimethoxyethane (DME) solvent before checking the scanning electron microscopy (SEM).

2.5. Electrochemical measurements

The electrochemical performance of Li-LFP batteries and Li–Li symmetrical cells were tested with CR2032 coin cells, constructed in an Ar-filled glove box with an external pressure of 35–40 kg cm^{-2}. The LFP cathode and patterned Li/bare Li anode were separated by a PEO electrolyte. The charge-discharge tests were carried out using a LAND CT-2001A system with voltages arrange from 2.7 V to 4.0 V at an operating temperature of 60 °C. Constant current densities were applied to the electrodes during the repeated Li stripping/plating process an operating temperature of 60 °C. Before testing, the Li–Li symmetric cells and Li-LFP full cells are kept in an 80 °C oven for overnight to the let PEO electrolyte well-wet both Li anode and LFP cathode.

The ionic conductivity of the electrolytes is determined by EIS measurement utilizing stainless steel | electrolyte | stainless steel symmetric cells with controlled temperatures.

3. Results and discussion

As shown in Fig. 1a, for the bare Li, there are many defects existed on the Li anode surface Fig. S1), resulting in and non-uniform charge distribution and Li dendrite growth during the plating/stripping process [28]. The Li dendrite easily penetrates the SPEs, here the most wildly used PEO electrolyte was chosen as the representative, thus leading to the occurrence of a short-circuiting and shortened cycling life of the ASSLBs. On the contrary, when creating a grid structure on the surface of Li metal and formed a patterned Li, as illustrated in Fig. 1b, the Li preferentially deposits in the grooves due to focused current density, thus suppressing the Li dendrite formation during the plating/stripping process [29]. With this in mind, the rational design of patterned Li has a great potential to improve the electrochemical performance SPEs-based ASSLBs.

The patterned Li is prepared by a template-press method, where a stainless steel mesh (SSM) acts as the template. As shown in Fig. S2, the units of the stainless steel present a diameter of around 50 μm. The schematic illustration is presented in Fig. 2a. Firstly, the SSM was put on the surface of a Li foil and then added an external pressure of 30 kg cm^{-2} and kept for 10s. As can be seen from the SEM images in Fig. S3, the SSM was partially pressed into the Li foil. After the SSM removal, a patterned Li that constructed with numerous 75 × 75 μm^2 square Li was obtained (Fig. 2b ~ d). According to the cross-sectional SEM images in Fig. 2e ~ g, the depth of the grooves among the square Li is determined to be around 100 μm. Due to the higher current density located at the grooves compared with the square Li, the Li preferentially deposits in the grooves, attributing to suppressed Li dendrite formation [29].

To identify the Li dendrite suppression capability of the as-prepared patterned Li in ASSLBs, the most widely used PEO electrolyte was chosen as the SSE. The morphology and structure of the PEO electrolyte are investigated by SEM. As shown in Fig. S4, the PEO electrolyte exhibits a flat surface with a thickness of around 160 μm. The ionic conductivity is determined to be 2.13 × 10^{-4} S cm^{-1} at an operating temperature of 60 °C (Fig. S5), which is in agreement well with recently reported pure PEO electrolytes [27,30,31].

The Li plating/stripping behaviors of patterned Li and bare Li are studied by the assembled Li–Li symmetrical cells (operating temperature: 60 °C), where a PEO electrolyte is sandwiched by two bare Li or patterned Li foils (diameter: 1.0 cm). The current densities are controlled as 0.1 mA cm^{-2} and 0.2 mA cm^{-2}, respectively, and each charging/discharging time is 1 h. As shown in Fig. 3a, due to the more fresh Li surface

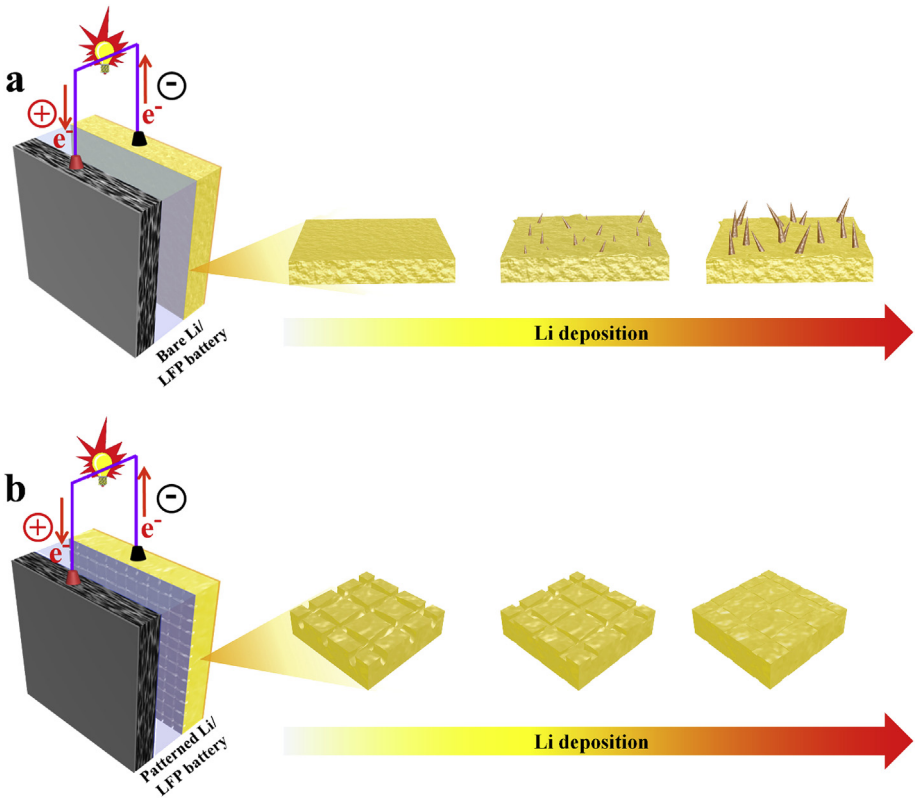

Fig. 1. Schematic illustration of the Li deposition process in (a) bare Li/LFP battery and (b) patterned Li/LFP battery.

available by the patterned Li, the assembled Li–Li symmetric cell delivers a stable overpotential of around 50 mV, which is almost 20 mV lower than the bare Li. More importantly, it is noteworthy to mention the cell assembled with PEO electrolyte displays intermittent short-circuiting after 82 h and complete short-circuiting after 149 h, which will result in safety issues and can't meet the demand of ASSLBs (Fig. 3b). The short-circuiting of Li–Li symmetric cells can be attributed to the poor mechanical properties of the PEO electrolyte, which isn't able to effectively

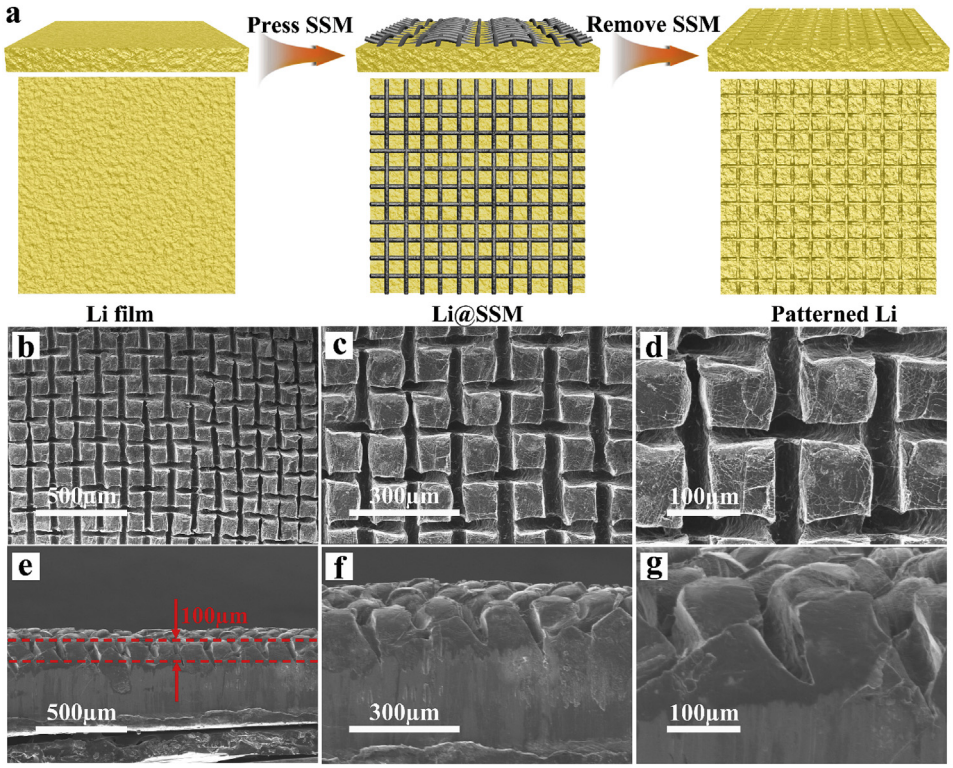

Fig. 2. (a) Schematic illustration of patterned Li fabrication. (b)~(d) surface and (e)~(g) cross-section morphology of patterned Li at different magnifications.

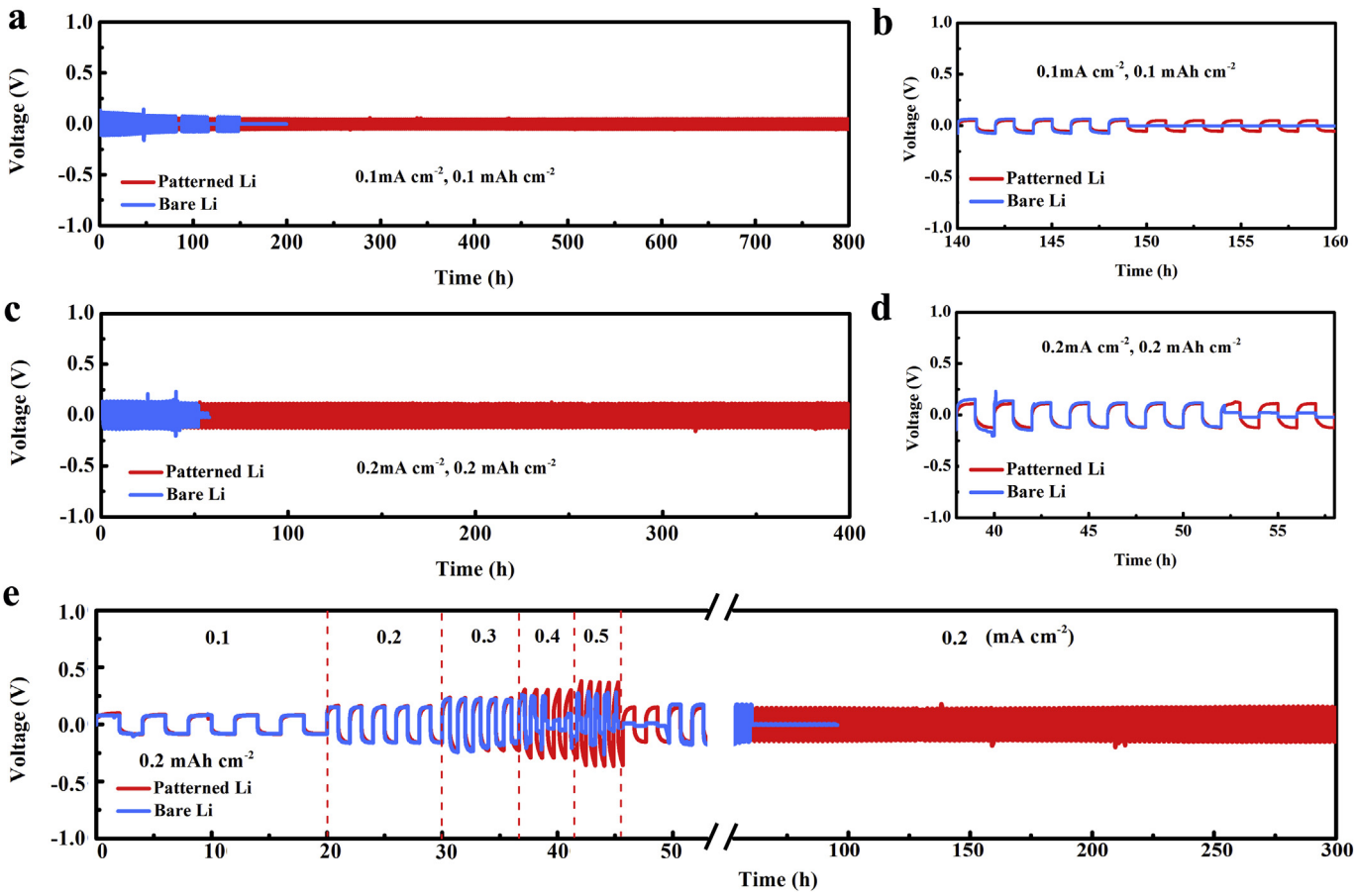

Fig. 3. Cycling stability of the Li–Li symmetrical cells assembled with patterned Li and bare Li at (a–b) 0.1 mA cm^{-2} (capacity: 0.1 mAh cm^{-2}) and (c–d) 0.2 mA cm^{-2} (capacity: 0.2 mAh cm^{-2}). (e) Rate performance of the Li–Li symmetrical cells assembled with patterned Li and bare Li at various current densities of 0.1–0.5 mA cm^{-2} with a limited capacity of 0.2 mAh cm^{-2}.

suppress Li dendrite because of non-uniform Li deposition during the plating/stripping process [24,27]. On the contrary, the Li–Li symmetric cell assembled with patterned Li presents excellent cycling stability with negligible overpotential change during 800 h plating/stripping process at 0.1 mA cm^{-2}.

When the current density is increased to 0.2 mA cm^{-2}, the overpotentials of the Li–Li symmetric cells assembled with the patterned Li and bare Li increase to around 107 mV and 138 mV, respectively, as shown in Fig. 3c. Considering the more serious Li dendrite growth at higher areal capacities and higher current densities, the cycling life of the cell assembled with bare Li further shortens to 52 h. After that, the occurrence of a short circuit is observed with the sharply reduced overpotential to around 0 V (Fig. 3d). Promisingly, the patterned Li-based Li–Li symmetric cell achieves stable cycling stability for over 400 h with slightly increased overpotential to 118 mV at an elevated current density of 0.2 mA cm^{-2}.

Meanwhile, as shown in Fig. 3e, the rate performance is also evaluated at various current densities from 0.1 to 0.5 mA cm^{-2}, while the capacity is controlled at a constant value of 0.2 mAh cm^{-2}. The Li–Li symmetric cell assembled with patterned Li presents very stable performance during the whole stripping/plating process with an overpotential of 365 mV at 0.5 mA cm^{-2} (Fig. S6a). In contrast, for the bare Li-based symmetric cell, a short-circuit is observed when the current density increases to over 0.4 mA cm^{-2} (Fig. 3g and Fig. S6b). Moreover, when the current density recovers to 0.2 mA cm^{-2}, the Li–Li symmetric cell assembled with patterned Li can still stably run for over 300 h, further highlighting the great capability of the patterned Li in suppressing Li dendrite.

To clarify the plating/stripping behavior within different Li anode, the Li–Li symmetrical cells operated at 0.2 mA cm^{-2} with different plating depths from 0.2 to 1.0 mAh cm^{-2} are disassembled and the morphology of Li anode are checked by SEM. As shown in Fig. 4ā c and Fig. 4e ~ g (the relative plating/stripping curves can be seen in Fig. 4i), surface SEM images demonstrate the selective Li deposition process in the grooves of patterned Li following Li plating. Furthermore, with plating depths increasing, more dense structure of Li was observed in the grooves when the capacity is increased from 0.2 to 1 mAh cm^{-2}. It should be noted that no obvious Li deposition is found on the surface of patterned Li even the grooves are full filled with Li (Fig. 4c, g), indicating the strong capability of patterned Li in suppressing Li dendrite growth. Interestingly, after stripping, the Li in the grooves disappeared and relieve the grooves for the next plating, which is meaningful to realize long cycling life of patterned Li (Fig. 4d, h). In contrast, for the bare Li, Li prefers to deposit along with the stripes due to ununiform charge distribution on the uneven surface (Fig. 4a'~c' and Fig. 4e'~g'). When the capacity increases 1 mAh cm^{-2} (Fig. 4c', g'), a Li dendrite net-work is presented. After stripping, as shown in Fig. 4d',h', the bare Li displays an uneven surface and some net-work Li is maintained. The irreversible Li plating/stripping process may be the main reason leads to the Li dendrite formation and short-life of Li–Li symmetric cells. The different Li plating behavior shown in Fig. 4 provides direct evidence to understand the prolonged cycling life of Li–Li symmetric cells with patterned Li anode and clarify the enhanced Li dendrite suppression capability of pattern Li.

The different Li dendrite suppression capabilities of the bare Li and patterned Li are further verified by the electrochemical performance of Li-LFP full ASSLBs. The cycling stability of Li-LFP ASSLBs assembled with patterned Li and bare Li, labeled as patterned Li/PEO/LFP and bare Li/PEO/LFP, respectively, are evaluated at galvanostatic charge/discharge

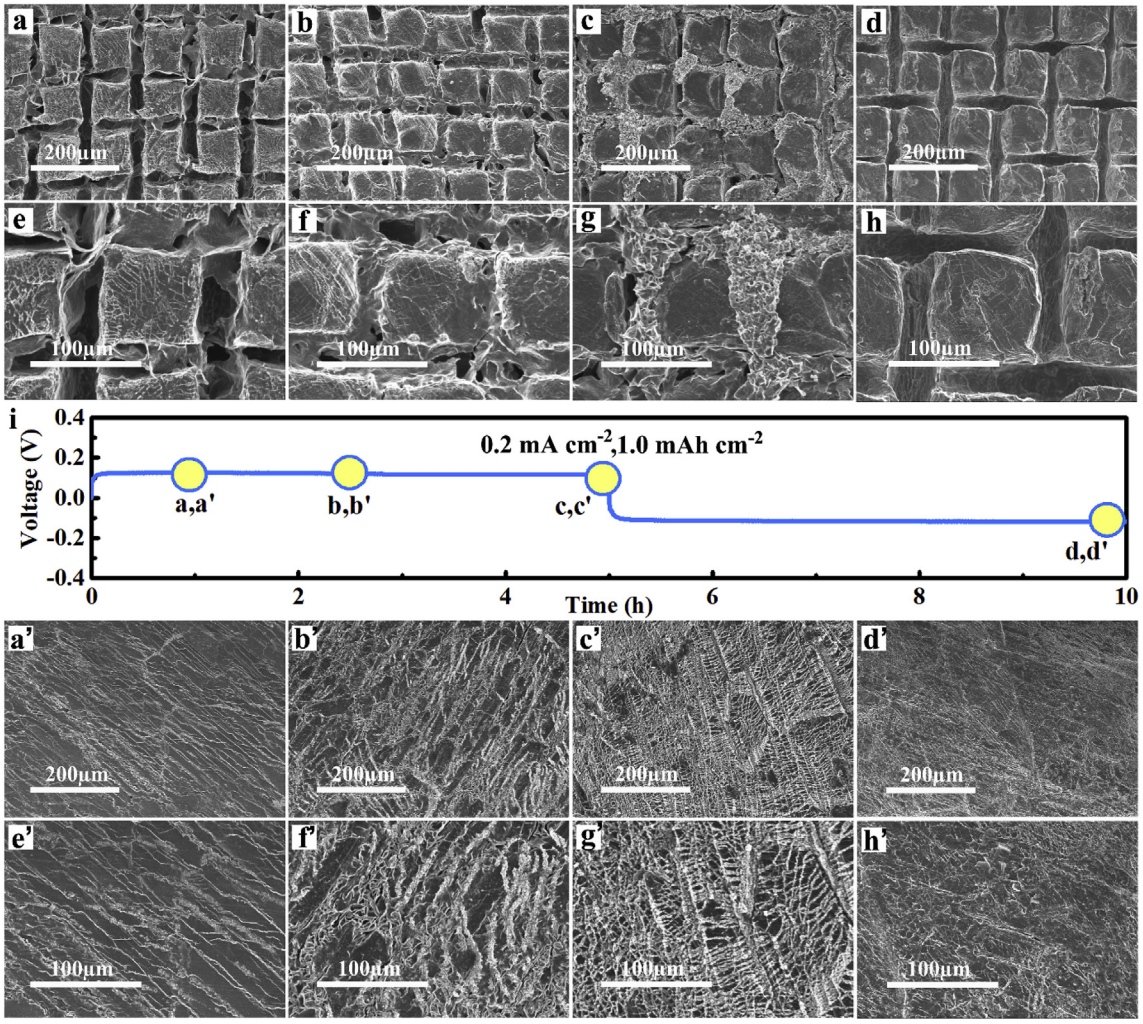

Fig. 4. SEM images of surface morphology evolution of patterned Li anode after (a,e) 0.2 mAh cm^{-2} (b,f) 0.5 mA h cm^{-2} (c,g) 1 mA h cm^{-2} of Li deposition, and (d,h) after one plating and stripping cycle after 1 mA h cm^{-2}. (i) The voltage profile indicated the Li plating and stripping states at a current density of 0.2 mA cm^{-2}, corresponding to (ãd and a'∼d').SEM images of surface morphology evolution of patterned Li anode after (a',e') 0.2 mAh cm^{-2} (b',f') 0.5 mA h cm^{-2} (c',g') 1 mA h cm^{-2} of Li deposition, and (d',h') after one plating and stripping cycle after 1 mA h cm^{-2}.

C-rates of 0.2C and 0.5C. As shown in Fig. 5a, at 0.2C, both cells exhibit an activation process in the first few cycles and then achieve reversible capacities around 160 mAh g^{-1}. In the 19th cycle, a sudden drop of Coulombic efficiency (CE) to around 50% can be observed for the bare Li/PEO/LFP cell, which attributes to the occurrence of short-circuiting. In contrast, the patterned Li/PEO/LFP cell maintains stable CEs of around 100% during the whole charging/discharging process and no short-circuiting phenomenon appeared. Moreover, even after 100 cycles, the patterned Li/PEO/LFP cell maintains a high capacity of 134 mAh g^{-1}, presenting excellent cycling stability. Considering that the same electrolyte and cathode are applied in the two cells, such a huge difference in CE and cycling life should be attributed to the different capabilities of Li anode in suppressing Li dendrite growth. To further highlight the Li dendrite suppression capability of patterned Li, the patterned Li (or bare Li)/PEO/LFP cells are further tested under a high C-rate of 0.5C, corresponding to current densities of around 0.26–0.34 mA cm^{-2}. As shown in Fig. 5b, similar to the performance at 0.2C, a reversible capacity of 138 mAh g^{-1}at the 8th cycle is delivered after an activation process. After 100 cycles, a high capacity of 126 mAh g^{-1} is retained, corresponding to a high capacity retention of 91.3%, demonstrating excellent cycling performance. Nevertheless, the bare Li/PEO/LFP cell can only stably run for 9 cycles and a sharp CE drop (37%) appear at the 10th cycle (Fig. 5d). The earlier short-circuit and lower CEs for bare Li/PEO/LFP can be attributed to the more serious Li dendrite growth under high current densities [32, 33].

The C-rate performance of patterned Li/PEO/LFP and bare Li/PEO/LFP cells are investigated under various C-rates from 0.1C to 0.8C. As shown in Fig. 5c, when the C-rate increases to 0.3C, there is a soft short-circuiting, confirmed by the fluctuating charge profile in Fig. 5f, occurred in the bare Li/PEO/LFP cell, where the CE slightly drop to 90% at the 12th cycle from over 98% at the 11th cycle. Further increasing the C-rate to 0.5C, more serious short-circuit and lower CEs are achieved. As displayed by the pink charge profile at 0.5C, a sudden voltage drop appears when the charging capacity is over 50 mAh g^{-1}, indicating the occurrence of a short-circuit, thus leading to lower CEs less than 30%. In other words, the PEO electrolyte is unable to effectively suppress the serious Li dendrite growth on the surface of bare Li, especially for the cells operating at high current densities. In contrast, during the whole C-rate performance testing, even with high C-rates over 0.8C, no short circuit phenomenon is observed and high CEs of around 100% are achieved for the patterned Li/PEO/LFP cell (Fig. 5c and e). The cell delivers average capacities of 162, 160, 155 and 142 mAh g^{-1} at 0.1, 0.2, 0.3 and 0.5C. Even at a high rate of 0.8C, a capacity of 110 mAh g^{-1} is still maintained.

The huge differences in electrochemical performance for both Li–Li symmetric cells and Li-LFP full cells highlight that the selective Li deposition strategy via designing a patterned Li is appreciated for the

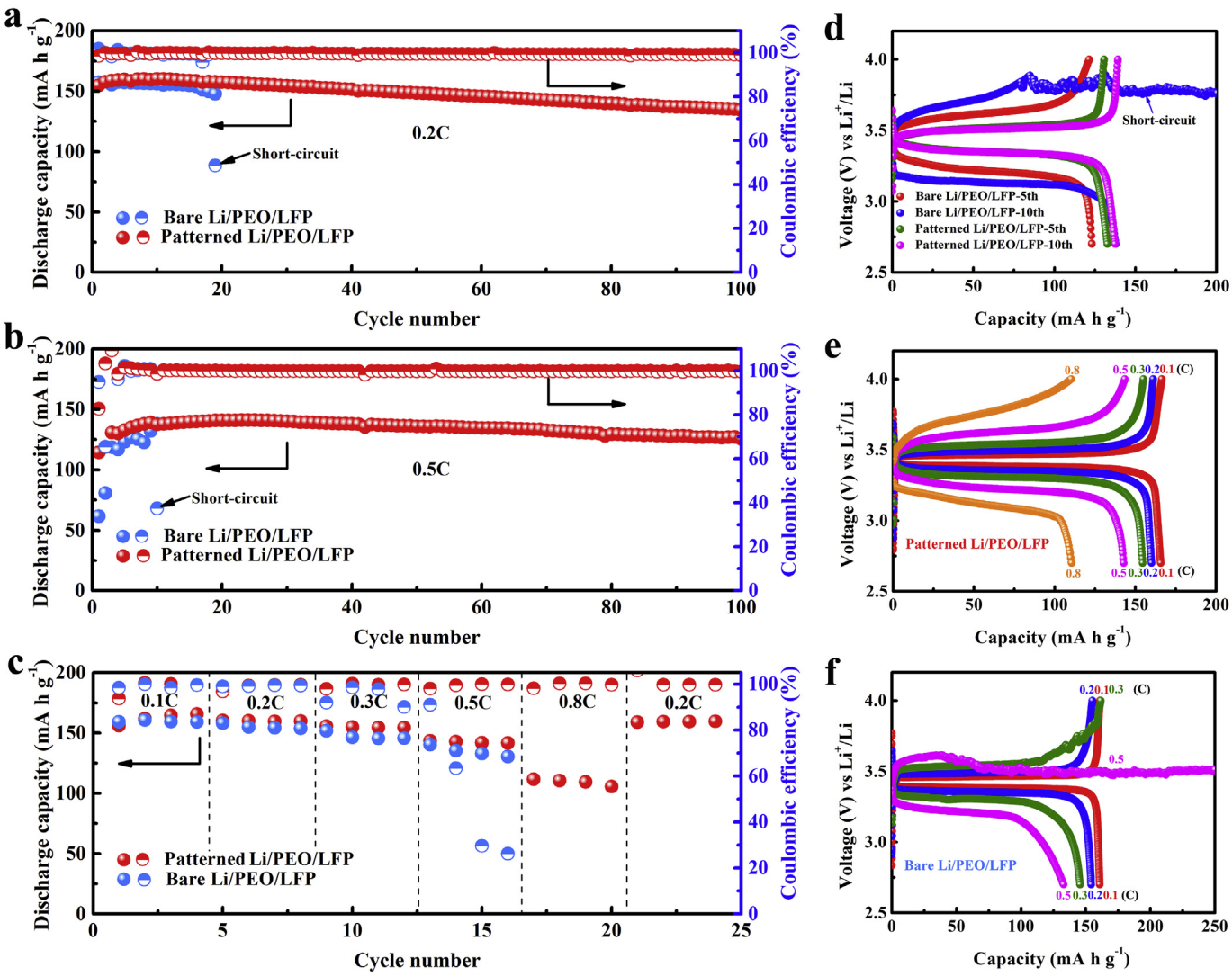

Fig. 5. Cycling performance at (a) 0.2C and (b) 0.5C of the bare Li/PEO/LFP and patterned Li/PEO/LFP cells. (c) C-rate performance of bare Li/PEO/LFP and patterned Li/PEO/LFP cells at various C-rate from 0.1C to 0.8C. (d) Charge-discharge profiles of bare Li/PEO/LFP and patterned Li/PEO/LFP cells at 0.5C for the 5th and 10th cycles. Charge-discharge profiles of (e) patterned Li/PEO/LFP and (f) bare Li/PEO/LFP cells at various C-rate. (All of the cells are tested at an operating temperature of 60 °C.)

improvement of Li dendrite suppression capability in ASSLBs. Considering the low-cost and facile manufactural process, this approach shows great potential to promote the practical application of ASSLBs.

4. Conclusion

In summary, we developed a selective Li deposition strategy to suppress Li dendrite formation in ASSLBs via rational designing a pattered Li. Due to the focused current density in the grooves, the Li preferentially deposits in the grooves rather than on the surface. Based on this concept, the Li–Li symmetric cells assembled with the pattered Li exhibit excellent cycling stability for 800 h (0.1 mA cm^{-2}, 0.1 mAh cm^{-2}) and 400 h (0.2 mA cm^{-2}, 0.2mAh cm^{-2}), respectively, which are over 5 times longer compared with their counterparts of bare Li. More importantly, the 3–4 mg cm^{-2} LFP-loaded patterned Li/PEO/LFP cells achieve a high capacity of 110 mAh g^{-1} at 0.8C and high capacity retention of 91.3% within 100 cycles at 0.5C, while different degrees of short-circuits occurred for the bare Li/PEO/LFP cells. Considering its facile and low-cost manufactural process, this strategy shows promising potential to be promoted to enhance the metal dendrite suppression capability in other solid-state batteries such as Li/Na–S and Li/Na–O_2 as well as Na-ion batteries.

Declaration of competing interest

The authors declare that they have no known competing financial interests or personal relationships that could have appeared to influence the work reported in this paper.

CRediT authorship contribution statement

Xiaofei Yang: Conceptualization, Writing - original draft. **Xuejie Gao:** Conceptualization, Writing - original draft. **Changtai Zhao:** Methodology. **Qian Sun:** Writing - review & editing. **Yang Zhao:** Methodology. **Keegan Adair:** Writing - review & editing. **Jing Luo:** Writing - review & editing. **Xiaoting Lin:** Formal analysis. **Jianneng Liang:** Formal analysis. **Huan Huang:** Software. **Li Zhang:** Validation. **Shigang Lu:** Validation. **Ruying Li:** Resources. **Xueliang Sun:** Supervision.

Acknowledgments

This work was partly supported by Natural Sciences and Engineering Research Council of Canada (NSERC), Canada Research Chair Program

(CRC), Canada Foundation for Innovation (CFI), Ontario Research Fund, China Automotive Battery Research Institute Co., Ltd, Glabat Solid-State Battery Inc. and University of Western Ontario. Qian Sun appreciates the support of MITACS Elevate postdoctoral program.

Appendix A. Supplementary data

Supplementary data to this article can be found online at https://doi.org/10.1016/j.ensm.2020.01.031.

References

[1] A. Manthiram, X. Yu, S. Wang, Nat. Rev. Mater. 2 (2017) 16103.
[2] Y. Zhao, K. Zheng, X. Sun, Joule 2 (2018) 2583–2604.
[3] E. Umeshbabu, B. Zheng, Y. Yang, Electrochem. Energy Rev. 2 (2019) 199–230.
[4] X. Yang, X. Li, K. Adair, H. Zhang, X. Sun, Electrochem. Energy Rev. 1 (2018) 239–293.
[5] H. Zhang, J. Zhang, J. Ma, G. Xu, T. Dong, G. Cui, Electrochem. Energy Rev. 2 (2019) 128–148.
[6] J. Liang, J. Luo, Q. Sun, X. Yang, R. Li, X. Sun, Energy Storage Mater. 21 (2019) 308–334.
[7] S.-J. Tan, X.-X. Zeng, Q. Ma, X.-W. Wu, Y.-G. Guo, Electrochem. Energy Rev. 1 (2018) 113–138.
[8] J. Zhang, J. Yang, T. Dong, M. Zhang, J. Chai, S. Dong, T. Wu, X. Zhou, G. Cui, Small 14 (2018), 1800821.
[9] H. Huo, J. Sun, C. chen, X. Meng, M. He, N. Zhao, X. Guo, J. Power Sources 383 (2018) 150–156.
[10] S. Liu, N. Imanishi, T. Zhang, A. Hirano, Y. Takeda, O. Yamamoto, J. Yang, J. Electrochem. Soc. 157 (2010) A1092–A1098.
[11] C. Wang, Y. Yang, X. Liu, H. Zhong, H. Xu, Z. Xu, H. Shao, F. Ding, ACS Appl. Mater. Interfaces 9 (2017) 13694–13702.
[12] X. Judez, H. Zhang, C. Li, G.G. Eshetu, Y. Zhang, J.A. Gonzalez-Marcos, M. Armand, L.M. Rodriguez-Martinez, J. Phys. Chem. Lett. 8 (2017) 3473–3477.
[13] D. Lin, W. Liu, Y. Liu, H.R. Lee, P.C. Hsu, K. Liu, Y. Cui, Nano Lett. 16 (2016) 459–465.
[14] L. Chen, Y. Li, S.-P. Li, L.-Z. Fan, C.-W. Nan, J.B. Goodenough, Nano Energy 46 (2018) 176–184.
[15] X. Tao, Y. Liu, W. Liu, G. Zhou, J. Zhao, D. Lin, C. Zu, O. Sheng, W. Zhang, H.W. Lee, Y. Cui, Nano Lett. 17 (2017) 2967–2972.
[16] H. Huo, Y. Chen, J. Luo, X. Yang, X. Guo, X. Sun, Adv. Energy Mater. (2019) 1804004.
[17] X. Ban, W. Zhang, N. Chen, C. Sun, J. Phys. Chem. C 122 (2018) 9852–9858.
[18] L. Liu, L. Chu, B. Jiang, M. Li, Solid State Ionics 331 (2019) 89–95.
[19] C.Z. Zhao, X.Q. Zhang, X.B. Cheng, R. Zhang, R. Xu, P.Y. Chen, H.J. Peng, J.Q. Huang, Q. Zhang, Proc. Natl. Acad. Sci. U.S.A. 114 (2017) 11069–11074.
[20] K.K. Fu, Y. Gong, J. Dai, A. Gong, X. Han, Y. Yao, C. Wang, Y. Wang, Y. Chen, C. Yan, Y. Li, E.D. Wachsman, L. Hu, Proc. Natl. Acad. Sci. U.S.A. 113 (2016) 7094–7099.
[21] D. Lin, P.Y. Yuen, Y. Liu, W. Liu, N. Liu, R.H. Dauskardt, Y. Cui, Adv. Mater. 30 (2018) 1802661.
[22] J. Bae, Y. Li, J. Zhang, X. Zhou, F. Zhao, Y. Shi, J.B. Goodenough, G. Yu, Angew. Chem. Int. Ed. Engl. 57 (2018) 2096–2100.
[23] K.K. Fu, Y. Gong, G.T. Hitz, D.W. McOwen, Y. Li, S. Xu, Y. Wen, L. Zhang, C. Wang, G. Pastel, J. Dai, B. Liu, H. Xie, Y. Yao, E.D. Wachsman, L. Hu, Energy Environ. Sci. 10 (2017) 1568–1575.
[24] X. Yang, Q. Sun, C. Zhao, X. Gao, K.R. Adair, Y. Liu, J. Luo, X. Lin, J. Liang, H. Huang, L. Zhang, R. Yang, S. Lu, R. Li, X. Sun, Nano Energy 61 (2019) 567–575.
[25] X.X. Zeng, Y.X. Yin, N.W. Li, W.C. Du, Y.G. Guo, L.J. Wan, J. Am. Chem. Soc. 138 (2016) 15825–15828.
[26] G.G. Eshetu, X. Judez, C. Li, O. Bondarchuk, L.M. Rodriguez-Martinez, H. Zhang, M. Armand, Angew. Chem. Int. Ed. Engl. 56 (2017) 15368–15372.
[27] X. Yang, Q. Sun, C. Zhao, X. Gao, K. Adair, Y. Zhao, J. Luo, X. Lin, J. Liang, H. Huang, L. Zhang, S. Lu, R. Li, X. Sun, Energy Storage Mater. 22 (2019) 194–199.
[28] F. Ding, W. Xu, G.L. Graff, J. Zhang, M.L. Sushko, X. Chen, Y. Shao, M.H. Engelhard, Z. Nie, J. Xiao, X. Liu, P.V. Sushko, J. Liu, J.G. Zhang, J. Am. Chem. Soc. 135 (2013) 4450–4456.
[29] J. Park, J. Jeong, Y. Lee, M. Oh, M.-H. Ryou, Y.M. Lee, Adv. Mater. Interfaces 3 (2016) 1600140.
[30] Y. Zhao, R. Tao, T. Fujinami, Electrochim. Acta 51 (2006) 6451–6455.
[31] O. Sheng, C. Jin, J. Luo, H. Yuan, C. Fang, H. Huang, Y. Gan, J. Zhang, Y. Xia, C. Liang, W. Zhang, X. Tao, J. Mater. Chem. 5 (2017) 12934–12942.
[32] H. Wang, D. Lin, Y. Liu, Y. Li, Y. Cui, Sci. Adv. 3 (2017), e1701301.
[33] Y. Zhao, X. Yang, Q. Sun, X. Gao, X. Lin, C. Wang, F. Zhao, Y. Sun, K.R. Adair, R. Li, M. Cai, X. Sun, Energy Storage Mater. 15 (2018) 415–421.